# Recognition and Classification of Wire Bonding Joint via Image Feature and SVM Model

Zhili Long, Xing Zhou, Xiaobing Zhang, Rui Wang, and Xiaojun Wu

*Abstract*—Recognition and classification for wire bonding joint are important to quality assurance in semiconductor device manufacturing. In this paper, a precision recognition and classification system for bonding joint of ultrasonic heavy aluminum wire based on image feature and support vector machine (SVM) is presented. This system consists of feature extraction from images and classification model. In feature extraction, image processing algorithms including Canny edge extraction, histogram equalization, and image morphology closed operation are utilized to extract and locate a joint contour in a complicated background image. In the classification model, the principal component analysis (PCA) is employed to visualize, reconstruct, and reduce the images data dimension for less computation time. The SVM-based model is chosen as the classifier to identify and recognize joint types. The Gauss-radial basis function (RBF) kernel function is adopted in SVM, and its optimal parameters are determined by cross-validation. In the experiment, 588 bonding images are used to implement in this recognition and classification system. The results prove that the classification accuracy for wire bonding joint based on image feature, PCA, and SVM can achieve to 97.3%, and the computation time can be reduced significantly.

*Index Terms*—Principal component analysis (PCA), recognition and classification, support vector machine (SVM) model, wire bonding joint.

## I. INTRODUCTION

**T**HE aluminum wedge bonding is an interconnection process to achieve electrical transport between the die and lead frame, where hybrid energy such as ultrasonic and pressure are applied simultaneously [1]–[3]. With the unique advantages of room temperature bonding and clean connection, the aluminum wedge bonding is widely applied to the microdevice packaging of products such as high-power modules and liquid crystal display modules [4]. In wedge bonding, the connection strength and intermetallic cover (IMC) of bonding joint are sensitive to not only bonding parameters such as ultrasonic power and bonding force but also to the equipment vibration and the location precision of the motion motors [5]. The abnormal factors in wire bonder would cause abundant failure or defect products in manufacturing. Therefore, it is significant to recognize or identify automatically the bonding quality in the wedge wire bonding.

Recognition and classification for wire bonding joint have attracted considerable attention from both researchers and manufacturers [6]–[9]. Currently, some approaches, including piezoelectric sensor, photoelectric sensor, force sensor, and vision sensor, have been developed to monitor the bonding quality. A common approach for monitoring the aluminum wire is to install a photoelectric sensor in the wire feeders to check whether the wire is lost. This industrial method is easy to implement, but the accuracy is low. Gual *et al.* [10] investigated the ultrasonic bonding *in situ* real-time amplitudes from a laser vibrometer and an integrated force sensor and found that the bonding process starts with a stiction phase, and thus, a clear break-off point can be found in the amplitude measurement. Or *et al.* developed a piezoelectric sensor in the ultrasonic transducer to measure the ultrasonic amplitude, which is calibrated to the bonding quality [11]. Long *et al.* [12] introduced a new monitoring approach by the Kalman filter and found that it is useful to monitor the wire errors. Recently, vision sensors have been more and more implemented in wire bonding due to their features of noncontact, high precision, and high speed.

Template matching, which is to compare and match a new joint area by using a standard image in advance, is a general algorithm to locate the joint area in wire bonding. However, the accuracy of the template-matching-based bonding joint quality inspection is low because the industrial images are often nonlinear and complex. Ieamsaard *et al.* [13] presented the detection methods with very high performance to detect solder ball joint defects on head gimbals assembly (HGA) including the vertical edge detection, chain code descriptor-based, and morphology and template-matching method. The morphology and template matching method for detection of solder ball bridging are compared with the chain code method [13]. Lee *et al.* [14] proposed a novel template-matching technique based on a genetic algorithm (GA) template matching (GATM), and the GA was used to determine the target position in the observed image efficiently and to select an adequate template image from several reference patterns for quick template matching.

Z. Long is with the Harbin Institute of Technology (Shenzhen), Shenzhen 518055, China, and also with the Key Laboratory of Precision Microelectronic Manufacturing Technology and Equipment, Ministry of Education, Guangdong University of Technology, Guangzhou 510006, China (e-mail: longzhili@hit.edu.cn).

X. Zhou, X. Zhang, R. Wang, and X. Wu are with the Harbin Institute of Technology (Shenzhen), Shenzhen 518055, China (e-mail: 960020310@qq.com; z_xiaobing@yeah.net; 475494210@qq.com; wuxj@hit.edu.cn).

As for the feature extraction and classification to the bonding joints, Zhang *et al.* [15] proposed a joint detection method based on the extreme learning machine (ELM) and least squares fitting, which achieved the bonding joint boundary extraction and joint defect classification. Said *et al.* [16] established an automatic defect identification and classification system for the detection of nonwet solder joints. This system consists of a region-of-interest (ROI) segmentation, feature extraction, reference-free classification, and automatic mapping [16]. In general, there are high dimension and redundant noise in image data set, which leads to huge calculation consumption. Therefore, the data preprocessing is indispensable to feature recognition and classification. Mar *et al.* [17] proposed two inspection modules for an automatic solder joint classification system. The "front-end" inspection system included illumination normalization, localization, and segmentation. The "back-end" inspection involved the classification of solder joints using the Log-Gabor filter and classifier fusion [17]. Kim [18] used the correlation values to classify the shape of the solder joint, and correlation values among all combinations of the 1-D vector sequences are computed and used for training an automatic solder joint shape classifier. Fan *et al.* [19] had presented an automatic recognition system of welding seam type based on the support vector machine (SVM). The proposed system can achieve welding seam-type recognition accuracy, and the computational cost can be reduced [19].

In summary, although some theoretical studies have investigated to bonding quality for wire bonding, its monitoring precision and calculation efficiency still need to be improved. In particular, automatic recognition with intelligent deep learning in wire bonding has rarely been reported. Current recognition of bonding joint is more limited to an empirical model. Therefore, it is essential to investigate the bonding quality recognition to achieve better precision and efficiency in wedge bonding.

Currently, the intelligent machining learning has gotten more and more applications in human face recognition, traffic classification, and robot navigation. In this paper, we propose some image processing methods to locate and extract bonding joint features. In order to decrease the computing time, we use principal component analysis (PCA) as a preprocessing algorithm to decrease the image dimensions. SVM, which is an intelligent machining learning algorithm, is utilized to classify the joint types. This paper is organized into five sections. Section II introduces the configuration of the ultrasonic wedge bonding system, where the vision module to attain the joint image is highly described. The location and extraction algorithm of the joint image are presented in Section III. Section IV shows the bonding joint classification, including PCA preprocessing and SVM classification. Finally, the conclusion is provided in Section V.

## II. System Configuration

### A. Process of Wedge Bonding

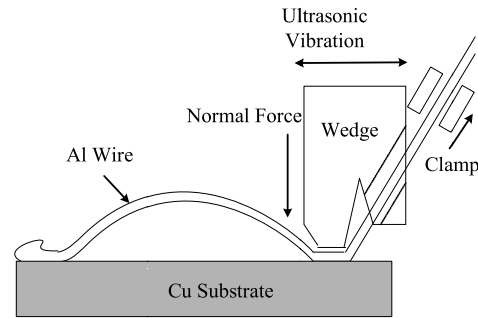The aluminum wedge bonding, as shown in Fig. 1, is a solid phase welding process in which two aluminum wires
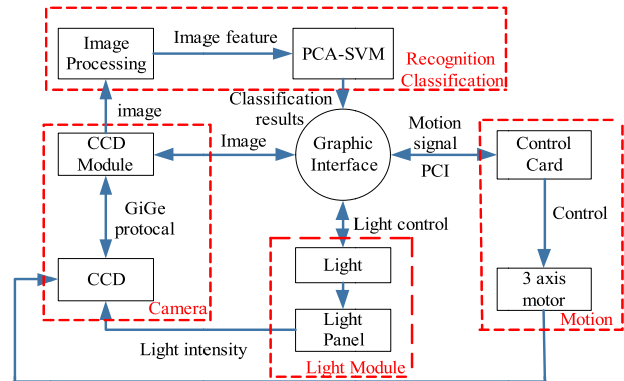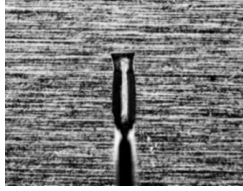


Fig. 1. Ultrasonic wedge bonding process.
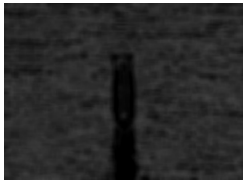


Fig. 2. Architecture of image acquisition and identification.

and a pad surface are brought into intimate contact. During the wire bonding process, the ultrasonic power and bonding force can result in material deformation that breaks up the contamination layer, smooth out surface asperity, accelerate atomic diffusion, and thus form the bonding connection. In our study, the ultrasonic power and frequency are set to 20.0 W and 60 kHz, respectively. The bonding force is 2.5 N, and the diameter of the aluminum wire is 100 $\mu$m.

### B. Vision System Configuration

The joint image of ultrasonic aluminum wire bonding is obtained by a vision sensor composed of a charge-coupled device (CCD). The vision sensor is important to joint feature exaction and recognition because the performance of the imag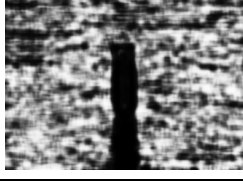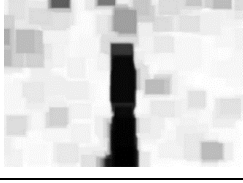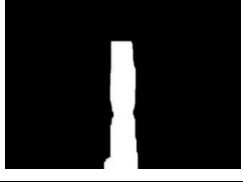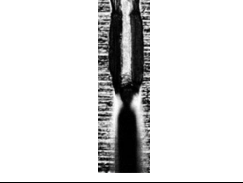e processing algorithms would be low if the sensor is inappropriate. In our study, the CCD vision sensor is chosen from German Imaging Source DMK-33G445 with $1280 \times 960$ at 30-frames/s resolution and 60-mm focal length of the lens. The light source is an eight-way LED light source control panel. We develop a graphical user interface (GUI) for image processing and joint feature recognition. Fig. 2 shows the architecture diagram for acquisition and identification of the joint image of wire bonding. In our study, 588 bonding joint images including 318 normal joint images and 270 defect joint images are collected for our analysis. Fig. 3 shows a group of typical joint image with normal and defect feature, respectively. It can be clearly observed that compared to the normal joint, the region of the defect joint is larger, the edge is not regular, and the surface is not smooth enough. There is lots of noise in the background, which makes the feature extraction difficult.

TABLE I

EXPRESSION, PARAMETER SETTING, AND RESULT OF EACH STEP FOR IMAGING PROCESSING

| Algorithm | Expression | Parameters | Result |
|---|---|---|---|
| Original images | $src = \begin{bmatrix} 12 & 23 & \cdot & \cdot & 56 \\ \cdot & & \cdot & \cdot & \cdot \\ \cdot & & \cdot & \cdot & \cdot \\ 24 & 35 & \cdot & \cdot & 53 \end{bmatrix}_{r \times c}$  <br> $r$ : image matrix rows, <br> $c$: image matrix columns. | $r=960$ <br> $c=1280$ |  |
| Average filter | $g(x,y) = \frac{1}{mn} \sum_{(s,t) \in S_{xy}} scr(s,t)$ <br> $S_{xy}$: image area center on $(x,y)$, <br> $m$, $n$: width and height of filter. | $m=5$ <br> $n=5$ |  |
| Canny edge extraction | $G_x = g(x,y) \otimes sobel_x$ <br> $G_y = g(x,y) \otimes sobel_y$ <br> Sobel: operator of edge detection. | $sobel_x = \begin{bmatrix} -1 & 0 & 1 \\ -2 & 0 & 2 \\ -1 & 0 & 1 \end{bmatrix}$ <br> $sobel_y = \begin{bmatrix} 1 & 2 & 1 \\ 0 & 0 & 0 \\ -1 & 2 & -1 \end{bmatrix}$ |  |
| Average filter after canny edge extraction | $I(x,y) = \frac{1}{mn} \sum_{(s,t) \in S_{xy}} G(s,t)$ <br> $S_{xy}$: image area center on $(x,y)$, <br> $m, n$ : width and height of filter. | $m=35$ <br> $n=35$ |  |
| Histogram equalization | $p(k) = \frac{n_k}{n}, k = 0,1,\cdots L-1$ <br> $H(i) = \sum_{j=0}^{i} p(j)$ <br> $p$: proportion of $k$ in image gray, <br> $H$ : total proportion less than $k$. | $L=255$ |  |
| Image morphology closed operation | $O(x,y) = H \bullet K$ <br> $K$: structural elements. | $K = (80, 80)$ |  |
| Inverse binarization | $dst(x,y) = \begin{cases} 0, & src(x,y) > thresh \\ 1, & otherwise \end{cases}$ <br> $thresh$: threshold used to inverse image. | $Thresh=90$ |  |
| Feature extraction result | $dst = \begin{bmatrix} 30 & \cdot & 56 \\ \cdot & & \cdot \\ \cdot & & \cdot \\ 68 & \cdot & 90 \end{bmatrix}_{r_1 \times c_1}$ <br> $r_1, c_1$: size of extracted joint image. | No constant value for $r_1$ and $c_1$. |  |

## III. FEATURE EXTRACTION OF BONDING JOINT

In order to attain the feature and contour of a bonding joint, the result can be regarded as the input data set of classification model. A seven-step image processing method, including average filter, Canny edge extraction [20], histogram equalization [21], image morphology, and inverse binarization, is proposed and implemented. In these algorithms, the Canny edge detection is selected to extract the edge of the joint
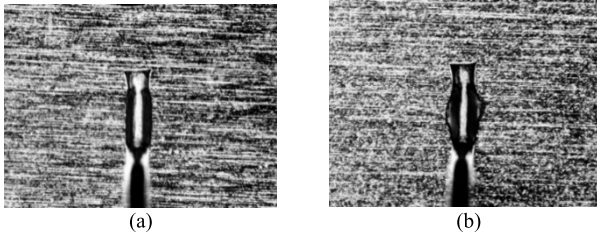
Fig. 3.   Typical joint image. (a) Normal joint. (b) Defect joint.



Fig. 4.   Contours merging for over segmentation. (a) Before merging. (b) After merging.

TABLE II

CONTOURS MERGING

| |
|---|
| **Input:** The contours of over segmented images. |
| **Process:** |
|    a) Calculating the pixel number of contours. |
|    b) Eliminating the contour less than 400 pixels. |
|    c) Eliminating the contours at the top of the joint image. |
|    d) Applying quadrilateral fitting on contours over 1200 pixels. |
|    e) Eliminating the contour at the top of the joint image. |
|    f) Merging the contours less than 1200 pixels. |
| **Output:** The region merged of joint image. |

image, histogram equalization is used to improve the contrast of the temporary image, and the closed operation of image morphology can eliminate the small holes in the images.

Table I summarizes the expressions, parameters setting, and result of each step of bonding joint extraction algorithm in our study.

As for the segmentation of joint images by the above image processing, some joints may be over segmentation such as the image shown in Fig. 4(a). In this case, contours merging algorithm in Table II is proposed to solve this problem, and the result images are shown in Fig. 4(b).

To verify the effectiveness of the proposed image processing algorithms for feature extraction, many images of different join contours are tested. Since the processing procedure for these images is the same, we present three groups of normal and defect joints as the example, and the results are shown in Fig. 5. It can be observed that the image feature of bonding joints can be accurately located and extracted by the proposed image processing algorithms.

## IV. PCA-BASED DATA PREPROCESSING

By the above image processing algorithms, the contour of a bonding joint is located and extracted. As to the extracted images, there still exists noise and redundant information in the image, which needs huge data computation and processing
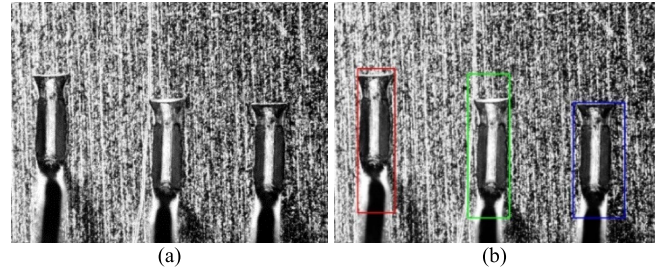


Fig. 5.   Feature extraction for multiple bonding joints. (a) Original image. (b) Extracted images.
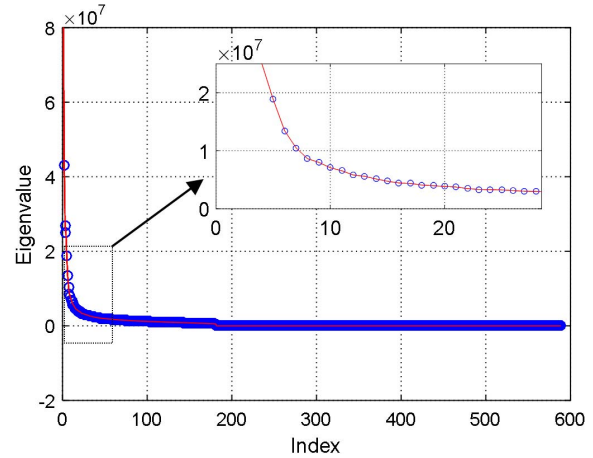


Fig. 6.   Eigenvalues distribution of extracted images.

time if without any preprocessing. In our study, a data preprocessing method on the basis of PCA is proposed to reduce and compress the data dimension and visualize the processing data. As a Karhunen–Loeve transformation, PCA has been widely used in the image reconstruction, data dimension reduction, and data visualization [22].

The data set of extracted bonding joint must be turned into a matrix before PCA processing. First, each extracted image of the bonding joint with the pixel dimension of $164 \times 639 = 104\,796$ is transformed to a 1-D array as an input sample $x_j$, and $x_j = [x_{j,1}, x_{j,2}, \ldots\ldots, x_{j,104\,796}]$. As shown in the following equation, the total original joint image data set is a matrix $D$ with 588 rows and $104\,796$ columns, where each row of the matrix represents a vector of the joint image:

$$D = \begin{bmatrix} x_{1,1} & x_{1,2} & \cdots & x_{1,104\,796} \\ x_{2,1} & x_{2,2} & \cdots & x_{2,104\,796} \\ \vdots & \vdots & \cdots & \vdots \\ x_{588,1} & x_{588,2} & \cdots & x_{588,104\,796} \end{bmatrix}. \qquad (1)$$

Table III demonstrates the procedure of the PCA algorithm for our bonding joint image dimension reduction. In our study, 588 extracted images are calculated by PCA, and their eigenvalues can be attained in Fig. 6. It is observed that the eigenvalue shows a sharp trend at low index such as 20th, where the eigenvalue is high from index 1 to 20, while it rapidly drops 0 after index 20th. It means that the first 20 principal eigenvalues contain the principal feature information of the data set. Therefore, we can select the percentage of the first $k$ principal eigenvalues to represent the

TABLE III

PCA DIMENSION REDUCTION

**Input**: Dataset $D=[x_1, \ x_2, \ ..., \ x_{588}]^T$,
$\quad\quad$ $k$: objective of reduction dimension.

**Process**:

$\quad\quad$ a) Centralize all samples $X = [x_1, x_2, \cdots x_{588}]^T$,

$$x_i \leftarrow x_i - \frac{1}{588}\sum_{j=1}^{588} x_j, \quad i = 1,2,\cdots 588,$$

$\quad\quad$ b) Compute the covariance matrix of dataset $X \cdot X^T$,
$\quad\quad$ c) Apply eigenvalue decomposition on covariance matrix,
$\quad\quad$ $\lambda_1 \geq \lambda_2 \geq \cdots \lambda_{588}$,
$\quad\quad$ d) Select the eigenvectors, $\omega_1, \omega_2, \cdots \omega_k$, corresponding to the first
$\quad\quad$ $k$ principal eigenvalues.

**Output**: The projection matrix: $W = [\omega_1, \omega_2 \cdots \omega_k]$,
$\quad\quad$ The vector after dimension reduction,
$\quad\quad\quad\quad$ $y_i = W^T \cdot (x_i - \overline{x}), \quad i = 1,2,\cdots 588$.

total eigenvalues, as

$$P_k = \frac{\sum_{i=1}^{k} \lambda_i}{\sum_{i=1}^{588} \lambda_i} \tag{2}$$

where $k$ is the principal component number of eigenvalues, representing the dimension of the reduced data set.

In order to verify the relationship between the dimension of reduced data set and image information, we use the inverse operation of PCA in the following expression to reconstruct the bonding joint image:

$$x_i = W \cdot y_i + \bar{x} \tag{3}$$

where $W$ is the projection matrix described in Table III, $\bar{x}$ is the mean of the data set. The reconstructed images of bonding joint with a different dimension of the reduced data set are listed in Table IV. It is proven that the image contour can be reconstructed successfully by the inverse PCA. When the eigenvalue percentage $P_k$ turns gradually from 20% to 95%, and the dimension of the reduced data set is chosen from 1 to 588, the contour of the bonding joint becomes more clearer, and the background becomes much more complicated. When the eigenvalue percentage $P_k$ reaches 95%, the original image can be completely recovered. It indicates that a different eigenvalue percentage represents a different sharpness of the joint image. Thus, it is feasible to make the balance between the image sharpness and eigenvalue percentage by an appropriate data set dimension, so as to reduce the noise and redundant information in an image.

## V. SVM MODELING

SVM is an excellent binary classification algorithm, which not only has a rigorous theoretical background but also can find the global optimal solutions. The introduction of the kernel function can make SVM to solve the nonlinear problems. Currently, SVM is widely applied for classification with small training, high dimensions [23]. In our investigation, the bonding joint images are captured by a CCD camera, and the contour location is extracted by certain image process algorithms. In order to reduce the computational cost, the

TABLE IV

RECONSTRUCTED JOINT IMAGES BY EIGENVALUE PERCENTAGE



| $P_2$=0.20 $k$=2 | $P_3$=0.30 $k$=3 | $P_5$=0.35 $k$=5 | $P_7$=0.40 $k$=7 | $P_{12}$=0.45 $k$=12 | $P_{18}$=0.50 $k$=18 |
|---|---|---|---|---|---|
| $P_{27}$=0.55 $k$=27 | $P_{41}$=0.60 $k$=41 | $P_{59}$=0.65 $k$=59 | $P_{84}$=0.70 $k$=84 | $P_{117}$=0.75 $k$=117 | $P_{159}$=0.80 $k$=159 |
| $P_{213}$=0.85 $k$=213 | $P_{283}$=0.90 $k$=283 | $P_{380}$=0.95 $k$=380 | $P_{588}$=1 $k$=588 | | |

dimension of joint images is reduced by PCA, and the result is regarded as the input data set of SVM classification.

### A. Mathematical Modeling of SVM

As a most common classifier, SVM aims to find a hyperplane $f(x) = \omega^T \phi(x) + b$ that maximizes the margin between the feature vectors of all samples data in the two classes. In order to solve the problem of overfitting, the slack variables $\xi_i$ are introduced. Moreover, SVM maps the training patterns from the input space $X$ to a high-dimensional feature space $F$, achieving the hyperplane to correctly classify all the samples. Thus, the mathematical model of SVM can be expressed as

$$\begin{cases} \min_{\omega,b,\xi_i} \ \frac{1}{2}\|\omega\|^2 + C\sum_{i=1}^{m} \xi_i \\ \text{s.t.} \ \ y_i(\omega^T \phi(x_i) + b) \geq 1 - \xi_i \\ \quad\quad \xi_i \geq 0, \quad (i = 1, 2, \ldots m) \end{cases} \tag{4}$$

where $C$ is a penalty factor to control the tradeoff between maximizing the margin and minimizing the training error. $\omega$
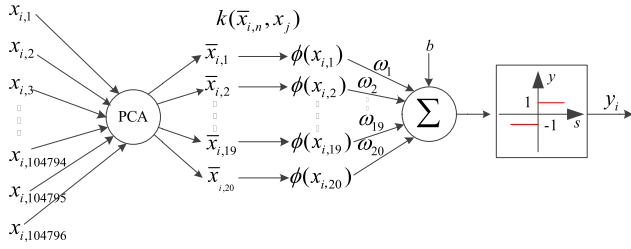
Fig. 7. Schematic of the SVM classification.

and $b$ present the trained weight and bias, respectively. $\phi : X \to F$ is a nonlinear map from the input space to the feature space. The schematic of the SVM classification is described in Fig. 7.

### B. Kernel Function

It is known that the data set of bonding joint images after dimension reduction is not linearly separable. Therefore, the kernel function $k(x_i, x_j)$ is introduced to solve the linear classification problem by computing the dot product of $k(x_i, x_j) = \phi(x_i)^T \phi(x_j)$. Currently, there are four typical kernel functions including linear, Gauss-radial basis function (RBF), sigmoid kernels, and polynomial convolution kernel. Because the Gauss-RBF is more suitable to classify the data set in high-dimensional space, it is chosen as the kernel function of SVM in our study. The Gauss-RBF kernel function is expressed as

$$k(x_i, x_j) = \exp\left(-\frac{(x_i - x_j)^2}{\gamma^2}\right) \tag{5}$$

where $\gamma$ has a relation to the number of support vector and determines the training time.

The hyperparameters $C$ and $\gamma$ are determined by a grid search by using cross-validation, whose main idea is that different parameter values are tested and the one with the best cross-validation accuracy is chosen [16]. Finally, the output of SVM is 0 or 1, representing the normal or defect bonding, respectively. Thus, a suitable SVM model of joint classification can be established, and the total flowchart of SVM system can be summarized in Fig. 8.

## VI. EXPERIMENTS AND RESULTS

A series of ultrasonic wire bonding experiments is carried out to verify the effectiveness of recognition and classification of the bonding joints. The bonding experiment is conducted in an automatic wire bonder by Wei xun WS9686 model, as shown in Fig. 9. The ultrasonic frequency for wire bond is 60 kHz, and the motion accuracy of the motor system is 10 $\mu$m in the $x$- and $y$-directions. The total of 588 joint images is divided into the training and testing sets. The training images are 500 including 274 normal images and 226 defect images. The testing images are 88 including half normal and half defect images, respectively. The main frequency of computer for SVM running is 3.0 GHz, and the RAM is 8 GB.

In order to prevent the data saturated by too large numbers, it is necessary to normalize the data set before SVM training. The maximum and minimum values of each item of the feature
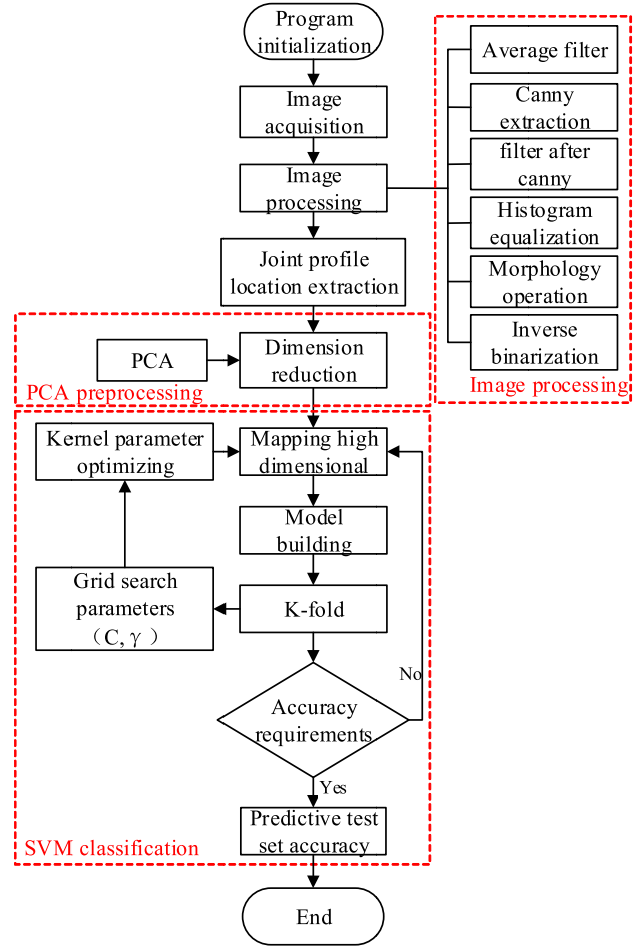


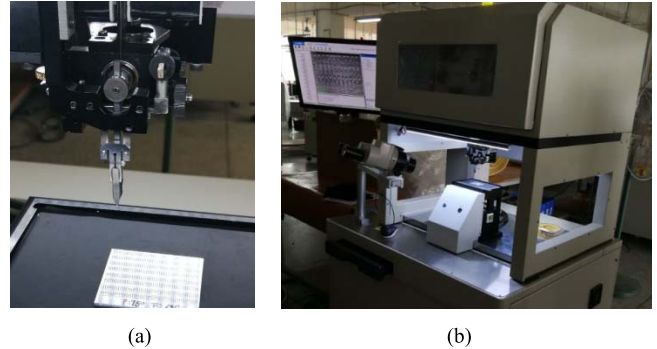Fig. 8. Flowchart of the SVM classification.



Fig. 9. Experimental platform. (a) Ultrasonic bonding head. (b) Bonding machine.

vector are calculated and reflected in the range of $[-1, 1]$. The expression is derived as

$$y = r_{\text{low}} + (r_{\text{high}} - r_{\text{low}}) \times \frac{x - x_{\min}}{x_{\max} - x_{\min}} \tag{6}$$

where $r_{\text{low}}$ is the lower limit after normalization, $r_{\text{high}}$ is the upper limit after normalization, $x_{\min}$ is the minimum value in the eigenvectors, and $x_{\max}$ is the maximum value in the eigenvectors.

The training of SVM is carried out by $K$-fold cross-validation, the grid search is used to search completely the hyperparameters $C$ and $\gamma$, and the result is shown in Table V.

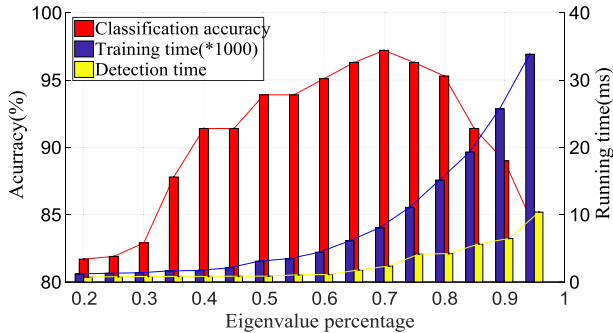| Hyper parameter | Minimum | Maximum | Optimal value |
|---|---|---|---|
| C | 0.1 | 500 | 2.50 |
| $1/\gamma^2$ | $10^{-5}$ | 0.6 | 5.0625 |



Fig. 10.    Accuracy of the SVM classification.

TABLE VI
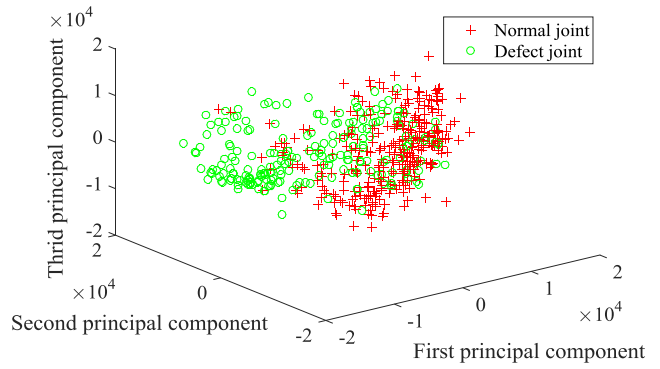
RESULT TO DIFFERENT EIGENVALUE PERCENTAGE

| $P_k$ | $k$ | $C$ | Classification accuracy (%) | Training time(s) | Detection time(ms) |
|---|---|---|---|---|---|
| 0.20 | 2 | 0.50 | 81.7 | 1.206 | 0.726 |
| 0.30 | 3 | 0.10 | 82.9 | 1.372 | 0.825 |
| 0.35 | 5 | 0.10 | 87.8 | 1.648 | 0.836 |
| 0.40 | 7 | 2.50 | 91.4 | 1.721 | 0.841 |
| 0.45 | 12 | 2.50 | 91.4 | 2.116 | 0.863 |
| 0.50 | 18 | 2.50 | 93.9 | 3.102 | 0.876 |
| 0.55 | 27 | 0.50 | 93.9 | 3.473 | 1.078 |
| 0.60 | 41 | 2.50 | 95.1 | 4.425 | 1.121 |
| 0.65 | 59 | 2.50 | 96.3 | 6.116 | 1.795 |
| 0.70 | 84 | 2.50 | 97.3 | 8.062 | 2.374 |
| 0.75 | 117 | 2.50 | 96.2 | 11.096 | 4.141 |
| 0.80 | 159 | 2.50 | 95.4 | 15.141 | 4.227 |
| 0.85 | 213 | 12.50 | 91.4 | 19.305 | 5.663 |
| 0.90 | 283 | 12.50 | 89.0 | 25.716 | 6.473 |
| 0.95 | 380 | 0.1 | 84.1 | 33.830 | 10.3851 |

The maximum and minimum values of hyperparameter are listed, and the optimal values $C = 2.50$ and $1/\gamma_2 = 5.0625$ are determined in our SVM model.

The SVM training is running by the procedure shown in Fig. 8. The classification accuracy of normal and defect bonding joint is shown in Fig. 10. It is found that when the eigenvalue percentage $P_k$ is 0.20, the classification accuracy is 82%, indicating that the projection data is insufficient to reflect the overall characteristics of the data set. When the eigenvalue percentage $P_k$ reaches 0.70, the classification accuracy turns up to 97.3%. Meanwhile, the classification accuracy turns lower when the eigenvalue percentage $P_k$ increases from 0.70 to 1, which may be caused by the redundant dimension of the data set. Therefore, the optimal eigenvalue percentage $P_k$ for the high accuracy and the joint image reconstruction can be attained as $P_k = 0.70$ and $k = 84$. It is also proved that the computational costing has been effectively saved and the dimension reduction has no negative influence to the training accuracy at data dimension $k = 84$, while the data dimension is 588 before dimension reduction.
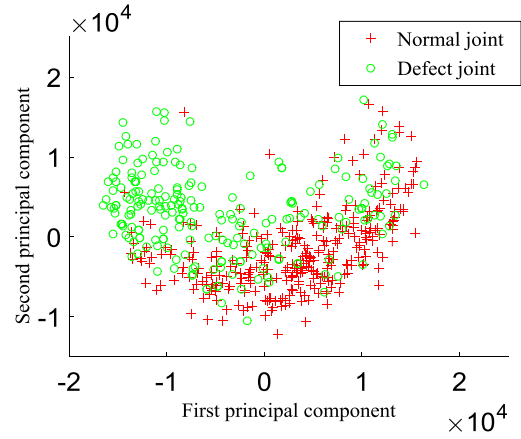


(a)



(b)

Fig. 11.    Data visualization by PCA. (a) $k = 2$. (b) $k = 3$.

Table VI lists the total parameters of SVM in the training and testing process. It is verified that when we chose a different eigenvalue percentage $P_k$ at PCA calculation, the data dimension and the parameter $C$ in SVM are different, which gives different computational time and classification accuracy. It is found that the testing and training time turns low effectively when the data dimension decreases. When the eigenvalue percentage $P_k = 0.70$, the training and testing time in SVM can turn to 8.062 s and 2.374 ms, compared to the 33.830 s and 10.3851 ms without the PCA dimension reduction. Fig. 11 demonstrates the data visualization when the data set dimension $k = 2$ and $k = 3$, respectively. It is proven that it is a nonlinear classification for the original normal and defect data, which is necessary to adopt the kernel function in SVM.

Traditionally, there were a few automatic means to inspect the bonding joint quality. In this paper, we proposed a novel, efficient, and automatic inspection method to check the quality of bonding joint based on the machine vision techniques. Compared with the other existing methods, only small image samples are used to train the classifier in our method. Therefore, the algorithm is very efficient and has high classification accuracy. With a small data set and high accuracy, it is believed that our method could be utilized in the practical applications.

## VII. CONCLUSION

In the IC or LED wire bonding process, an effective joint recognition system is necessary for high reliability and perfor-

mance of electronic products. In this paper, an identification and classification system to wire bonding joint is presented via image feature extraction and SVM intelligent machine learning. The conclusions can be drawn as follows. The configuration of the CCD vision system is established to capture the bonding joint images. The components of the vision system are described, and 588 original joint images are captured. The contour and feature of the bonding joint are extracted and located by seven images processed such as the Canny edge extraction, histogram equalization, and image morphology closed operation. A contour merging algorithm is developed to solve the segmentation of joint images. In order to reduce the dimension of the image data set and save the computational time, PCA algorithm is introduced to compress the redundant information. The relationship between the reduced dimension and images sharpness is discussed. SVM is used to classify the normal and defect bonding joint. The Gauss-RBF kernel is chosen to solve the nonlinear classification to the image data set. The experiment proves that the classification accuracy to the bonding joint can be 97.3%, when the data set dimension is reduced to 84 from the original 588. The training and testing time in PCA and SVM can turn to 8.062 s and 2.374 ms, compared to the 33.830 s and 10.3851 ms without dimension reduction. As our method proves to be highly accurate and easy to use, it is possible to employ the proposed method in practical applications. In the future, we will make our method more general to different kinds of solder joint and conduct more practical applications.

## References

[1] R. R. Tummala, *Microelectronics Packing Handbook*. New York, NY, USA: Kluwer, 2001.

[2] F. L. Wang, J. H. Li, S. H. Liu, and L. Han, "Heavy aluminum wire wedge bonding strength prediction using a transducer driven current signal and an artificial neural network," *IEEE Trans. Semicond. Manuf.*, vol. 27, no. 2, pp. 232–237, May 2014.

[3] Z. Long, L. Han, Y. Wu, and J. Zhong, "Study of temperature parameter in au–ag wire bonding," *IEEE Trans. Electron. Packag. Manuf.*, vol. 31, no. 3, pp. 221–226, Jul. 2008.

[4] F. Wang, H. Zhang, C. Liang, Y. Tian, X. Zhao, and D. Zhang, "Design of high-frequency ultrasonic transducers with flexure decoupling flanges for thermosonic bonding," *IEEE Trans. Ind. Electron.*, vol. 63, no. 4, pp. 2304–2312, Apr. 2016

[5] F. Wang *et al.*, "A novel actuator-internal micro/nano positioning stage with an arch-shape bridge type amplifier," *IEEE Trans. Ind. Electron.*, to be published. doi: 10.1109/TIE.2018.2885716.

[6] D. Zhang and S. F. Ling, "Monitoring wire bonding via time-frequency analysis of horn vibration," *IEEE Tran. Electron. Packag. Manuf.*, vol. 26, no. 3, pp. 216–220, Jul. 2003.

[7] W. Feng, Q. f. Meng Y. Xie, and H. Fan, "Wire bonding quality monitoring via refining process of electrical signal from ultrasonic generator," *Mech. Syst. Signal Process.*, vol. 25, pp. 884–900, Apr. 2011.

[8] Y. Bar-Cohen, X. Bao, Z. Chang, and S. Sherrit, "An ultrasonic sampler and sensor platform for *in-situ* astrobiological exploration," *Proc. SPIE*, vol. 5056, pp. 5055–5056, Aug. 2003.

[9] F. Wang, J. Li, S. Liu, X. Zhao. D. Zhang, and Y. Tian, "An improved adaptive genetic algorithm for image segmentation and vision alignment used in microelectronic bonding," *IEEE/ASME Trans. Mechatronics*, vol. 19, no. 3, pp. 916–923, Jun. 2014.

[10] H. Gaul, M. Schneider-Ramelow, and H. Reichl, "Analytic model verification of the interfacial friction power in Al us w/w bonding on Au pads," *IEEE Trans. Compon. Packag. Technol.*, vol. 33, no. 3, pp. 607–613, Sep. 2010.

[11] S. W. Or, H. L. W. Chan, and C. K. Liu, "Piezocomposite ultrasonic transducer for high-frequency wire-bonding of microelectronics devices," *Sens. Actuators A, Phys.*, vol. 133, pp. 195–199, Jan. 2007.

[12] Z. Long, Y. Zheng, C. Li, and Y. He, "Wire loss monitoring in ultrasonic wedge bonding using the Kalman filter algorithm," *IEEE Trans. Compon. Packag. Manuf. Technol.*, vol. 6, no. 1, pp. 153–160, Jan. 2016.

[13] J. Ieamsaard and T. Fuangpian, "Automated optical inspection for solder jet ball joint defects in the head gimbal assembly process," in *Visual Inspection Technology in the Hard Disk Drive Industry*. Berlin, Germany: Springer-Verlag, 2015, pp. 99–129.

[14] Y. Lee, T. Hara, H. Fujita, S. Itoh, and T. Ishigaki, "Automated detection of pulmonary nodules in helical CT images based on an improved template-matching technique," *IEEE Trans. Med. Imag.*, vol. 20, no. 7, pp. 595–604, July. 2001.

[15] C. Zhang and H. Liu, "The detection of bonding joint defect and solar panel orientation based on elm and robust least square fitting," in *Proc. Control Decis. Conf.*, May 2011, pp. 561–565,

[16] A. F. SAID, B. L. Bennett, L. J. Karam, and J. S. Pettinato, "Automated detection and classification of non-wet solder joints," *IEEE Trans. Autom. Sci. Eng.*, vol. 8, no. 1, pp. 67–80, Jan. 2011.

[17] N. S. S. Mar, P. K. D. V. Yarlagadda, and C. Fookes, "Design and development of automatic visual inspection system for PCB manufacturing," *Robot. Comput. Integr. Manuf.*, vol. 27, no. 5, pp. 949–962, Oct. 2011.

[18] J. H. Kim, "Method and apparatus for inspecting a solder joint using a correlation neural network," U.S. Patent 6 404 206 B1, Mar. 3, 2000.

[19] J. F. Fan, F. S. Jing, Z. J. Fang, and M. Tan, "Automatic recognition system of welding seam type based on SVM method," *Int. J. Adv. Manuf. Technol.*, vol. 92, no. 4, pp. 989–999, Sep. 2017.

[20] J. Canny, "A computational approach to edge detection," *IEEE Trans. Pattern Anal. Mach. Intell.*, vol. PAMI-8, no. 6, pp. 679–698, Nov. 1986.

[21] C. A. M. Jaspers, "Histogram equalization," U.S. Patent 6 741 736, Jan. 1, 2004.

[22] M. E. Tipping and C. Bishop, "Probabilistic principal component analysis," *J. Roy. Stat. Soc. B, Stat. Methodol.*, vol. 21, no. 3, pp. 611–622, 2010.

[23] M. M. Adankon and M. Cheriet, "Support vector machine," in *Encyclopedia of Biometrics*, S. Z. Li and A. Jain, Eds. Boston, MA, USA: Springer, 2009.

**Zhili Long** received the B.S., M.S., and Ph.D. degrees in mechatronics engineering from Central South University, Changsha, China, in 2000, 2002, and 2007, respectively.

He is currently an Associate Professor with the Department of Mechatronics, Harbin Institute of Technology, Shenzhen, China. His current research interests include the process analysis of ultrasonic packaging, and model and optimization of an ultrasonic actuator.
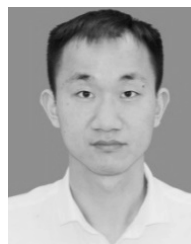
**Xing Zhou** is currently pursuing the master's degree with the Department of Mechatronics, Harbin Institute of Technology, Shenzhen, China.

His current research interests include the machining learning in wire bonding.
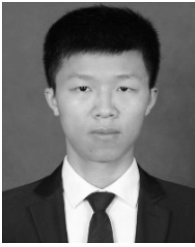
**Xiaobing Zhang** is currently pursuing the master's degree with the Department of Mechatronics, Shenzhen Graduate School, Harbin Institute of Technology, Shenzhen, China.

His current research interests include the machining learning in robot.
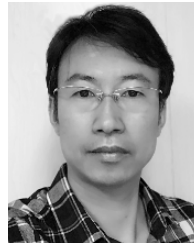
**Xiaojun Wu** received the B.S. and M.S. degrees from Jilin University, Changchun, China, in 1994 and 1998, respectively, and the Ph.D. degree from the Shenyang Institute of Automation, Chinese Academy of Sciences, Beijing, China, in 2001.

He is currently an Associate Professor with the Harbin Institute of Technology, Shenzhen, China. His current research interests include machine vision in electronic packaging.

**Rui Wang**, photograph and biography not available at the time of publication.